Facilitation and restoration of cognitive function in primate prefrontal cortex by a neuroprosthesis that utilizes minicolumn-specific neural firing



2012 J. Neural Eng. 9 056012

(http://iopscience.iop.org/1741-2552/9/5/056012)

J. Neural Eng. **9** (2012) 056012 (17pp) doi:10.1088/1741-2560/9/5/056012

# Facilitation and restoration of cognitive function in primate prefrontal cortex by a neuroprosthesis that utilizes minicolumn-specific neural firing

**Robert E Hampson[1], Greg A Gerhardt[2], Vasilis Marmarelis[3], Dong Song[3], Ioan Opris[1], Lucas Santos[1], Theodore W Berger[3] and Sam A Deadwyler[1,4]**

[1] Department of Physiology and Pharmacology, Wake Forest University School of Medicine, Winston-Salem, NC, USA
[2] Department of Anatomy and Neurobiology, University of Kentucky, Lexington, KY, USA
[3] Department of Biomedical Engineering, University of Southern California, LA, CA, USA

E-mail: sdeadwyl@wfubmc.edu

Received 22 May 2012
Accepted for publication 7 August 2012
Published 13 September 2012
Online at stacks.iop.org/JNE/9/056012

**Abstract**

*Objective*. Maintenance of cognitive control is a major concern for many human disease conditions; therefore, a major goal of human neuroprosthetics is to facilitate and/or recover the cognitive function when such circumstances impair appropriate decision making. *Approach*. Minicolumnar activity from the prefrontal cortex (PFC) was recorded from nonhuman primates trained to perform a delayed match to sample (DMS), via custom-designed conformal multielectrode arrays that provided inter-laminar recordings from neurons in the PFC layer 2/3 and layer 5. Such recordings were analyzed via a previously demonstrated nonlinear multi-input–multi-output (MIMO) neuroprosthesis in rodents, which extracted and characterized multicolumnar firing patterns during DMS performance. *Main results*. The MIMO model verified that the conformal recorded individual PFC minicolumns responded to entrained target selections in patterns critical for successful DMS performance. This allowed the substitution of task-related layer 5 neuron firing patterns with electrical stimulation in the same recording regions during columnar transmission from layer 2/3 at the time of target selection. Such stimulation improved normal task performance, but more importantly, recovered performance when applied as a neuroprosthesis following the pharmacological disruption of decision making in the same task. *Significance*. These findings provide the first successful application of neuroprosthesis in the primate brain designed specifically to restore or repair the disrupted cognitive function.

(Some figures may appear in colour only in the online journal)

## Introduction

Performance deficits related to cognitive dysfunction are in many cases characterized by the inability to employ the appropriate behavioral response in circumstances in which choice changes routinely as a function of task-dependent complexity (Shallice and Burgess 1991, Duncan *et al* 1997, Beveridge *et al* 2008, Buxhoeveden *et al* 2006, Dobbs 2010, Brennan and Arnsten 2008, Wang *et al* 2011). According to many theories of cognition, cortical executive

[4] Author to whom any correspondence should be addressed.

 

decision mechanisms coordinate and control 'online' cognitive processes underlying behavioral selection, working memory, behavioral inhibition and multi-tasking (Posner and Snyder 1975, Shallice and Burgess 1996, Goldman-Rakic 1996, Miyaki *et al* 2000 Baddeley 2002, Miller and Cohen 2001, Graybiel 2008). Disruption of the normal functional status of the prefrontal cortex (PFC) which utilizes precise minicolumnar organization of neural firing to coordinate attention, decision making and movement selection can lead to failure in cognitive performance for several reasons since this proposed microcircuitry consists of neurons in the supra-granular layers (L2/3), that integrate sensory signals and communicate directly with cells in the infra-granular layers (L5) in prefrontal (area 46) and frontal cortical regions (areas 6 and 8) (Buxhoeveden *et al* 2006, Buxhoeveden and Casanova 2002). However, since the microanatomic basis for information processing in this region is similar in terms of minicolumnar inter-laminar connectivity, restoration of the lost function could be achieved by the duplication of patterned layer 5 outputs based on previous inputs from layer 2/3 cells over the same minicolumnar structure (Kritzer and Goldman-Rakic 1995, Hasselmo 2005, Opris *et al* 2011). In this paper, we provide evidence for the existence of such 'executive microcircuitry' within the PFC, featuring cortical minicolumns (Mountcastle 1997, Weiler *et al* 2008, Opris *et al* 2011, Takeuchi *et al* 2011) that coordinate activity in nonhuman primates (NHPs) required to make behavioral decisions to evaluate and respond to an appropriate target.

In order to implement a previously successful multi-input–multi-output (MIMO) dynamic nonlinear neural prosthesis model for the recovery of function and cognitive capability (Berger *et al* 2012, Hampson *et al* 2012a, Hampson *et al* 2012b, Berger *et al* 2011), a selective pharmacologic disruption of PFC columnar processing was produced which resulted in decreased cognitive performance, mimicking cortical malfunction similar to that characterized in many human disease states (Casanova *et al* 2008, van Veluw *et al* 2012, Tomasi *et al* 2010, Buxhoeveden *et al* 2006). Application under these conditions provided the means to test the MIMO model utilizing the interposed delivery of device-extracted patterns of task-successful multicolumnar firing via electrical stimulation to the same areas. Such stimulation was employed on a trial-by-trial basis to reverse the pharmacologic state of depressed inter-laminar transmission during the decision and selection stages of the task. The results provide the first instance of the application of neuroprosthesis designed specifically for the recovery of cognitive processing in the primate brain by restoring columnar activation patterns, and as such indicate a potential efficacy for application to cortical dysfunction related to many types of human diseases (Casanova *et al* 2008, van Veluw *et al* 2012, Casanova *et al* 2010, Kusunoki *et al* 2010, Grabenhorst *et al* 2008, Buxhoeveden *et al* 2006).

## Methods

### *Experimental subjects*

All animal procedures were reviewed and approved by the Institutional Animal Care and Use Committee of Wake Forest University, in accordance with US Department of Agriculture, International Association for the Assessment and Accreditation of Laboratory Animal Care and National Institutes of Health guidelines. Five NHP subjects (rhesus, *Macaca mulatta*) were trained to perform a version of the delayed-match-to-sample (DMS) task (Hampson *et al* 2004b) for juice rewards to a criterion performance level that was stable for at least one year.

### *Visual delayed-match-to-sample (DMS) task*

NHPs utilized ($n = 5$) were trained to perform the well-characterized, custom-designed visual DMS task (Deadwyler *et al* 2007, Porrino *et al* 2005, Hampson *et al* 2011, Hampson *et al* 2004b) shown in figure 1(A). During task performance, animals were seated in a primate chair with a shelf-counter in front of them facing a large display screen (figure 1(A)). Right arm position on the counter top was tracked via a UV-fluorescent reflector attached to the back of the wrist which was illuminated with a 15 W UV lamp and detected by a small LCD camera positioned 30 cm above the hand. Hand position and movement were digitized and displayed as a bright yellow cursor on the projection screen and horizontal positions of illuminated targets were computed from the video image using a Plexon Cineplex scanner connected to a behavioral control computer. Trials were initiated by the animal placing the cursor inside a yellow 3″ diameter circle 'Start signal' displayed in the center of the screen. This was followed by a clip-art image displayed in the sample phase to be selected in the match phase among other images on that same trial. Following trial initiation, a single unique image was displayed randomly on the screen (sample image) and constituted the Sample phase of the task which required placement of the cursor into the image (sample response) to initiate the next phase, the delay interval in which the screen was blanked for 1–90 s on a trial-to-trial basis. Termination of the delay interval was signaled by the onset of the screen display in the match phase of the task in which 2–7 trial unique images, including the sample image, were presented at separate randomly selected spatial locations on the screen as shown in figure 1(A). Placement of the cursor into the sample image constituted the correct 'match response' (MR) which blanked the screen and produced a drop of juice delivered via a sipper tube located near the animal's mouth. Placement of the cursor into one of the non-match (distracter) images constituted a non-match-error response and caused the screen to blank without reward delivery. Trials were separated by a minimum of 10 s in which the start signal (circle) was presented following the termination of the match phase of the prior trial. All images (samples and distracters) were unique for each trial over the entire session (100–150 trials) and were selected randomly from an image reservoir ($n = 5000$) updated every month (Hampson *et al* 2004b). All subjects were trained to overall performance levels of 70–75% correct on the least difficult trials with graded declines in performance on trials with increased delays and number of images in the match phase of the task (figure 1(A)).

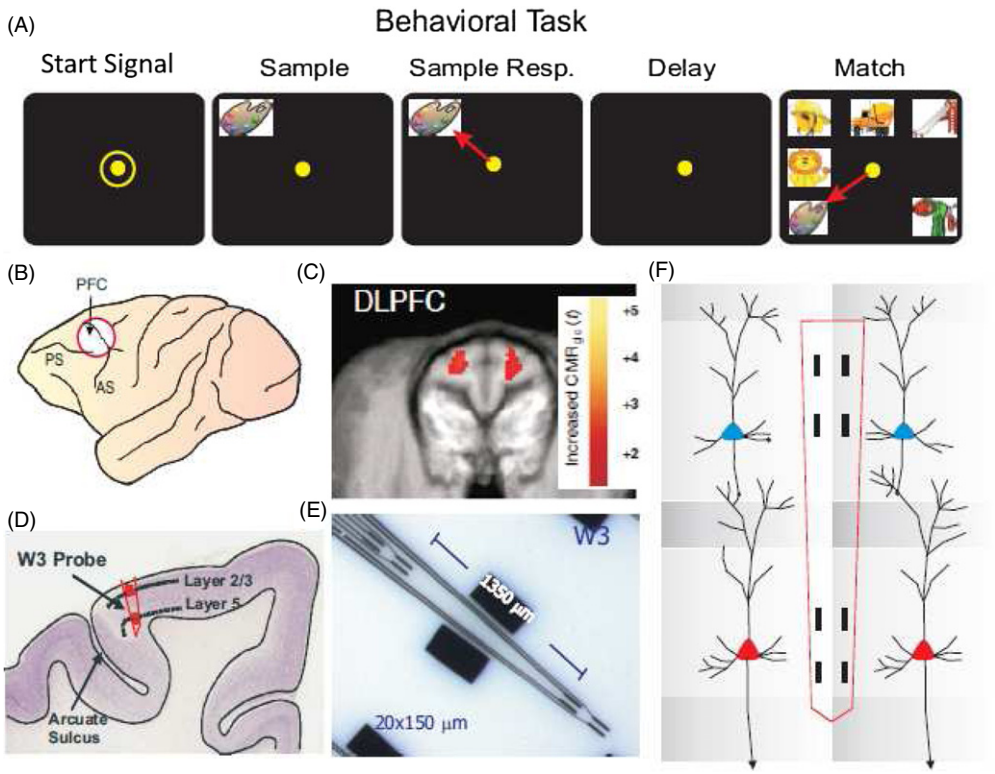


**Figure 1.** Illustration of behavioral task and prefrontal cortical recording localization. (A) Behavioral paradigm showing the sequence of events in the DMS task. (1) 'Focus ring' presentation and response to initiate the trialcommencing with (2) presentation of the 'sample target' image, followed by (3) 'sample response' by cursor movement into the image which initiates (4) variable 'delay' period of 1–90 s prior to (5) the presentation of the 'match' target (sample image) accompanied by 1–6 non-match (distracter) images on the same screen. Cursor movement into correct (match target) image for 0.5 s was rewarded by juice reward (0.5 ml) via a sipper tube next to the animal's mouth. Placement of the cursor into a non-match image for 0.5 s caused the screen to blank without reward delivery. Intertrial interval (ITI): 10.0 s. (B) Diagram of NHP brain showing PFC recording locations (accessing cortical areas 46, 8, 6). (C) Representative magnetic resonance image (MRI) of coronal section through DLPFC centered on the area in (B). PET-imaged localized cerebral metabolic rate (LCMRglu) activation (red blots) indicates metabolic activity of DLPFC during DMS task performance (Hampson *et al* 2011; Porrino *et al* 2007). (D) Illustrated histologic section of DLPFC brain showing relative location of supra-granular layer 2/3 (L2/3) and infra-granular layer 5 (L5) with tract (in red) used for placement of conformal MEA recording (W3) probes shown in (E). (E) Ceramic conformal recording array custom designed (W3) for inter-laminar and inter-columnar cortical recording (diagram in (F)) consisting of dual sets of four recording pads vertically aligned and separated by 1350 $\mu$m the anatomic distance between L2/3 and L5 in primate brain.
(F) Dimensionally relevant illustration of the conformal MEA positioned for simultaneous recording from neurons in both layers in adjacent minicolumns (1 and 2), each minicolumn consisting of a 'pair' of L2/3 and L5 PFC cells.

*Surgery*

Animals were surgically prepared with cylinders for attachment of a microelectrode manipulator over the specified brain regions of interest. During surgery animals were anesthetized with ketamine (10 mg kg$^{-1}$), and then intubated and maintained with isoflurane (1–2% in oxygen 6 l min$^{-1}$). Recording cylinders (Crist Instruments, Hagerstown, MD) were placed over 20 mm diameter craniotomies for electrode access (Hampson *et al* 2011, Opris *et al* 2011) to stereotaxic coordinates of the frontal cortex (25 mm anterior relative to interaural line and 12 mm lateral to midline/vertex) in the caudal region of the principal sulcus, the dorsal limb of arcuate sulcus in area 8 and the dorsal part of the premotor area 6 (figures 1(C) and (D)), areas previously shown by PET imaging to become activated during task performance (figure 1(E)) (Porrino *et al* 2005). Two titanium posts were secured to the skull for head restraint with titanium screws embedded in bone cement. Following surgery, animals were given 0.025 mg kg$^{-1}$ buprenorphine for analgesia and penicillin to prevent infection. Recording cylinders were disinfected three times weekly with betadine during recovery and daily during recording. Vascular access ports (Norfolk Medical Products, Skokie, IL) for drug infusions were implanted subcutaneously in the mid-scapular region, the end of the catheter threaded subcutaneously to a femoral incision, inserted into the femoral vein, threaded for a distance calculated to terminate in the vena cava and flushed daily with 5 ml heparinized saline needed for IV drug administration.

*Electrophysiological recording*

Electrophysiological procedures and analysis utilized the 64-channel MAP Spike Sorter by Plexon, Inc. (Dallas, TX). Recordings from the PFC were obtained with a custom-designed conformal ceramic multielectrode array (MEA) manufactured in collaboration with Dr Greg Gerhardt (Center for Microelectrode Technology—CenMet, Lexington, KY)

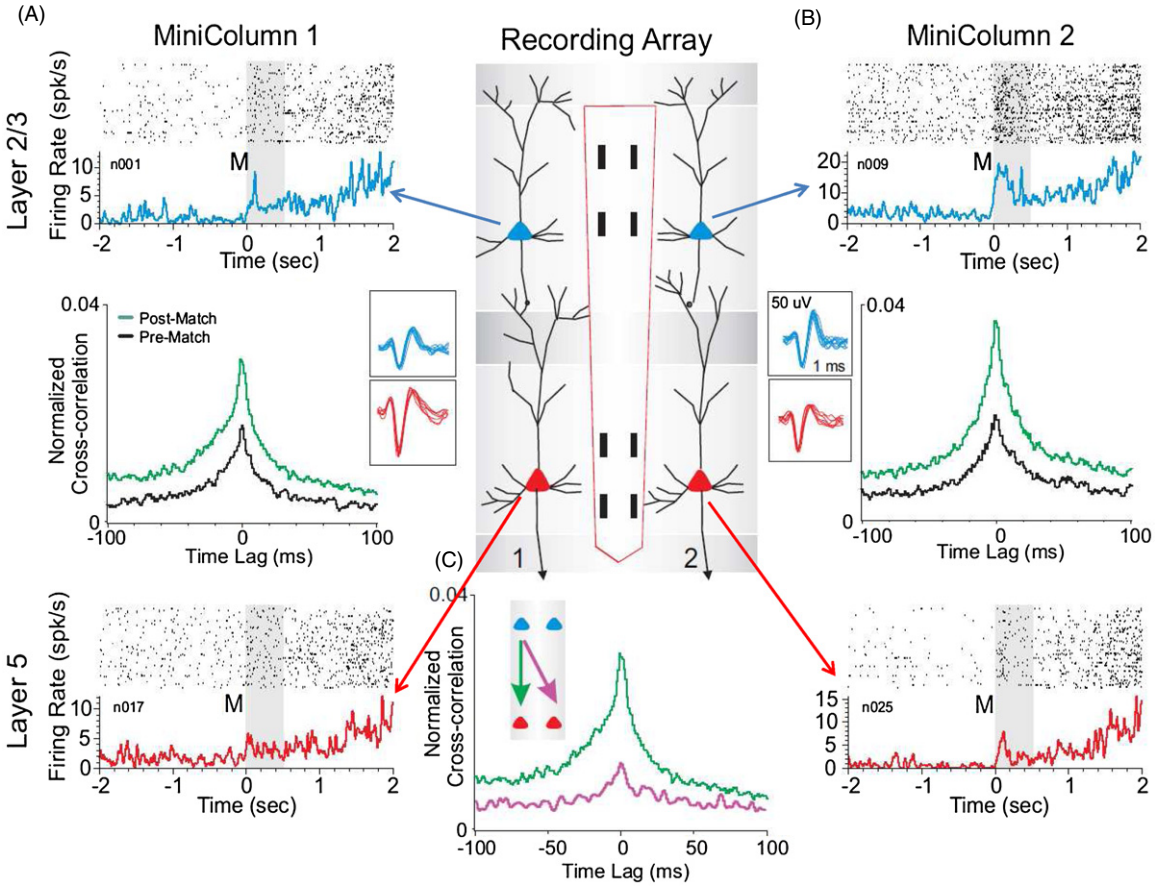


**Figure 2.** Coherence of inter-laminar activity within but not between adjacent prefrontal minicolumns during DMS task performance. The center panel shows the conformal multielectrode recording array (MEA) positioned for simultaneous inter-laminar columnar recording from adjacent minicolumns 1 and 2 (40 $\mu$m separation) with L2/3 and L5 cell pairs (figure 1(F)) shown as the corresponding (blue and red) cell waveforms. (A) and (B) show corresponding cell data as individual trial rasters and average PEHs obtained from two cell pairs recorded simultaneously from L2/3 (blue) and L5 (red) within the respective minicolumns. Rasters and PEHs depict $\pm 2.0$ s relative to match phase (figure 1(A)) onset (0.0 s) within a single DMS session. Cross-correlation histograms (CCHs) for the same cell pairs within each minicolumn are shown in the middle of the raster-PEH displays. The CCHs display increased inter-laminar synchronization during target selection (green) during the match phase (0.0+2, 0 s, post) relative to similar correlations between the same cell pairs constructed 2.0 s prior to onset ($-2.0$ s to 0.0 s in PEHs) of the match phase (black, pre). (C) Examples of post-match phase CCHs in which L2/3 and L5 cell pairs were localized to (1) the same (minicolumn 1, green arrow) or (2) diagonally via different minicolumns (i.e. L2/3 minicolumn 1, L5 minicolumn 2 purple arrow) which was not significant ($F_{(1,401)} < 3.22$, $p > 0.10$) show the specificity of MEA columnar orientation. Post-match CCHs for cell pairs from all types of diagonal comparisons on the same MEA across different minicolumns were previously reported (Opris *et al* 2011).

at the University of Kentucky (Moxon *et al* 2004). MEAs consisted of etched platinum pads (figure 1(E)) constructed for recording isolated single neuron extracellular action potentials on specifically aligned recording pads (figure 2) during events within DMS trials (Opris *et al* 2011). The MEA probe (figure 1(E)) was specially designed to conform to the columnar anatomy of the PFC such that the top four recording pads (separated by 40 $\mu$m horizontally and 100 $\mu$m vertically) recorded activity from neurons in the supra-granular layer 2/3 (L2/3), while the lower set of four pads, separated vertically by 1300 $\mu$m in terms of probe orientation in the PFC, simultaneously recorded neurons in the infra-granular layer 5 (L5) as shown in figure 1(F). This pad configuration ensured that only cells in L2/3 and L5 were isolated, since the appearance of cells simultaneously on both vertically separated sets of pads required 0° angular orientation relative to both cell layers (Takeuchi *et al* 2011) as shown in figure 1(D).

*Data analysis*

Task performance was determined for each animal ($n = 5$) as per cent correct trials within and across sessions and related to simultaneous recordings of multiple MEA conformal single neuron firings during match phase image selection on individual trials (Hampson *et al* 2011) in the DMS task (figure 1(A), match phase). Cell types were identified as regular firing PFC cells in terms of the baseline (nonevent) firing rate (Opris *et al* 2009, 2011) and significant changes ($z > 3.09$, $P < 0.001$) in firing (see below) on single trials in perievent histograms (PEHs) derived for intervals of $\pm 2.0$ s relative to the onset of the screen image display (0.0 s) in the match phase of the task (figure 2). Task-related neural activity was classified according to locations on the conformal MEA positioned in L2/3 and L5 (figure 1(F)) upon insertion in the PFC prior to the start of the DMS session. Standard scores, $z =$ (peak – baseline firing rate)/SD baseline firing rate, were

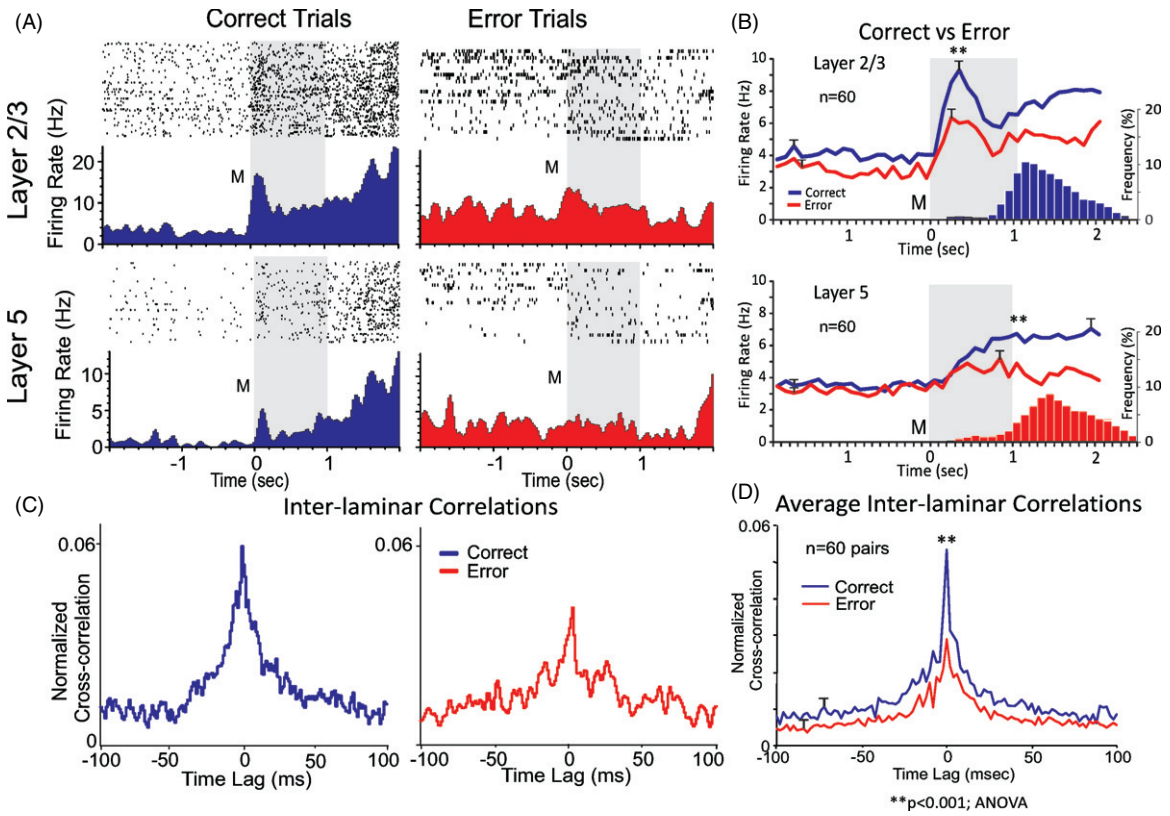


**Figure 3.** Differences in PFC columnar processing on correct versus error trials. (A) Match phase rasters and PEHs recorded from a L2/3 (upper) and L5 (lower) cell pair within a single minicolumn, segregated as to correct (blue) and error (red) trials during a single session ($n =$ 120 trials). (B) Line graphs represent mean match phase PEHs averaged over all recorded inter-laminar PFC cell pairs ($n = 60$), L2/3 (upper) and L5 (lower), on correct (blue) versus error trials (red) summed across animals and sessions. No more than two cell pairs were recorded in same behavioral session from the same MEA. Blue (correct) and red (error) bar graphs show the associated mean frequency distributions of match response latencies for the same associated correct and error trials plotted on the same time-base as the PEHs relative to match phase onset (0.0 s). (C) Coherent intralaminar activity of L2/3 and L5 neuron pair segregated by correct and error trials as in (A). CCHs indicate respective correct and error trial paired neural firing during first 1.0 s after match presentation (M, time = 0.0 s above). (D) Normalized cross-correlograms of match phase firing (figure 2) between the same pair of (L2/3 and L5) cells for correct (blue) versus error (red) trials during same session shown in (A). (D) Tuning plots (as in figure 3(B)) constructed for same pair of cells shown in (A) on correct (blue) versus error (red) trials. Tuning bias = 135° for both cells. (E) Mean cross-correlation histograms CCHs for the same inter-laminar cell pairs ($n = 60$) shown in (B) constructed from correct (blue) and error (red) trials. $^{**}F_{(1,401)} = 14.18$, $p < 0.001$.

calculated for individual cell firing on each DMS task event (Hampson *et al* 2004b). The firing rate for simultaneously recorded L2/3 and L5 neurons was analyzed in 100 ms bins over ± 2.0 s relative to the time of initiation (0.0 s) of the match phase (figure 2). Neurons were only included in the analysis if their firing rates were significantly elevated (*Z*-scores, ANOVA F test $p < 0.01$) relative to the same time interval prior to match screen presentation (−2.0–0.0 s).

### *Identification of cortical layers and minicolumns*

The conformal MEA probe (figure 1(E)) was designed such that the two sets of vertical recording pads detected simultaneous activity from neurons separated by 1300 $\mu$m, which, given the perpendicular orientation of insertion to the cell layers in the PFC (dorsal premotor gyrus in area 6, stereotactic coordinates AP:25 and ML:12), consisted of cells in the supra-granular layer 2/3 (L2/3) and infra-granular layer 5 (L5) as shown in figure 1(F) (Hampson *et al* 2004a, Gold and Shadlen 2007, Opris *et al* 2005a, 2005b, Casanova *et al* 2010). The MEAs (Hampson *et al* 2010, Opris *et al* 2011, Moxon *et al* 2004), therefore all the recording of PFC columnar activity from two different adjacent sets of pads which permitted assessment and validation via correlation between inter-laminar cell pairs recorded on the same probe in distinct minicolumns (Takeuchi *et al* 2011, Hansen and Dragoi 2011, Mo *et al* 2011) as shown in figure 2(C). Statistical analyses also determined whether there were inter-laminar differences in firing rates during activation in the match phase for cells in different layers (i.e. L2/3 versus L5). Differences in cross-correlation were assessed using normalized distributions of coefficients extracted from firing of inter-laminar cell pairs under different conditions related to the performance in the match phase of the task (figures 2, 3, 7). Normalized mean coefficients were used to construct cross-correlation histograms (CCHs) which satisfied 99% confidence limits requirement for the comparison of the same cell pairs under different experimental conditions (Opris *et al* 2011). The correspondence of firing between cells in different layers was tested via CCHs employing L2/3

cell firing to test synchronous discharge with simultaneously recorded L5 cells in 1.0 ms intervals over ± 1.0–2.0 s time of occurrence of task-related events (figure 2(C)). CCHs for interlaminar cell pairs (L2/3 and L5) were generated using a shift-predictor (http://www.neuroexplorer.com/), which computed cross-correlation levels due to random simultaneous spike occurrences and eliminated these from the true coefficients for CCHs to adjust for differences in cell firing rates and frequency of bursting (Opris *et al* 2011, Takeuchi *et al* 2011). Population CCHs were computed by averaging coefficients across multiple cell pairs and plotting the mean values (± SEM) in 1.0 ms bins (figures 3 and 7).

*Application of the MIMO model to PFC columnar processing*

In prior studies (Hampson *et al* 2012b, Berger *et al* 2011), it has been shown that a MIMO nonlinear dynamic model applied to spatiotemporal patterns of multiple recordings from synaptically connected neurons is capable of extracting patterns of firing related to the successful task performance which can then be used to facilitate and recover the performance when administered to the same locations as patterns of electrical pulses (Hampson *et al* 2012a, Berger *et al* 2011). This type of general Volterra kernel-based nonlinear model has been applied in other formats which have also been shown to be effective in rodents (Marmarelis *et al* 2011). The MIMO version of the model was applied here to the minicolumnar data recorded by the conformal MEA probes in the animals performing the DMS task described here (figures 1 and 2). The MIMO model was applied here as modeling strategy for the nonlinear dynamics underlying spike-train-to-spike-train transformations between L2/3 and L5 which was established to predict L5 output firing patterns from input patterns of L2/3 neural activity as a representation of multicolumnar firing patterns (Berger *et al* 2012, Hampson *et al* 2012a, Berger *et al* 2011, Song *et al* 2009, Song *et al* 2007, Berger *et al* 2005). In this application, the identification of spatio-temporal pattern transformations from the PFC layer 2/3 to layer 5 in MEA identified columns was formulated as the estimation of a MIMO model, decomposed into a series of multi-input single-output (MISO) models with the physiologically identifiable structure expressed by the following equations:

$$w = u(k, x) + a(h, y) + \varepsilon(\sigma), \quad y = \begin{cases} 0 & \text{when } w < \theta \\ 1 & \text{when } w \geqslant \theta \end{cases}$$

The variable $x$ represents input spike trains and $y$ represents output spike trains. The hidden variable $w$ represents the pre-threshold membrane potential of the output neurons and is equal to the summation of three components, i.e. the post-synaptic potential $u$ caused by the input spike trains, the output spike-triggered after-potential $a$ and a Gaussian white noise $\varepsilon$ with standard deviation $\sigma$. The noise term models both the intrinsic noise of the output neuron and the contribution of unobserved inputs. When $w$ exceeds threshold, $\theta$, an output spike is generated and a feedback after-potential ($a$) is triggered and then added to $w$. Feedforward kernels $k$ describe the transformation from $x$ to $u$. The feedback kernel, $h$, describes the transformation from $y$ to $a$. $u$ can be expressed as a Volterra functional series of $x$:

$$\begin{aligned} u(t) = k_0 &+ \sum_{n=1}^{N}\sum_{\tau=0}^{M_k} k_1^{(n)}(\tau)x_n(t-\tau) \\ &+ \sum_{n=1}^{N}\sum_{\tau_1=0}^{M_k}\sum_{\tau_2=0}^{M_k} k_{2s}^{(n)}(\tau_1,\tau_2)x_n(t-\tau_1)x_n(t-\tau_2) \\ &+ \sum_{n_1=1}^{N}\sum_{n_2=1}^{n_1-1}\sum_{\tau_1=0}^{M_k}\sum_{\tau_2=0}^{M_k} k_{2x}^{(n_1,n_2)}(\tau_1,\tau_2)x_{n_1}(t-\tau_1)x_{n_2}(t-\tau_2) \\ &+ \sum_{n=1}^{N}\sum_{\tau_1=0}^{M_k}\sum_{\tau_2=0}^{M_k}\sum_{\tau_3=0}^{M_k} k_{3s}^{(n)}(\tau_1,\tau_2,\tau_3) \\ &\times x_n(t-\tau_1)x_n(t-\tau_2)x_n(t-\tau_3) + \cdots. \end{aligned}$$

The zeroth-order kernel, $k_0$, is the value of $u$ when the input is absent. First-order kernels, ${k_1}^{(n)}$, describe the linear relation between the $n$th input $x_n$ and $u$. Second- and third-order self-kernels, ${k_{2s}}^{(n)}$ and ${k_{3s}}^{(n)}$, describe the second- and third-order nonlinear relation between the $n$th input $x_n$ and $u$, respectively. Second-order cross-kernels ${k_{2x}}^{(n1,n2)}$ reflect the second-order nonlinear interactions between each unique pair of inputs ($x_{n1}$ and $x_{n2}$) as they affect $u$. $N$ is the number of inputs. $M_k$ denotes the memory length of the feedforward process. The feedback variable $a$ can be expressed as

$$a(t) = \sum_{\tau=1}^{M_h} h(\tau)y(t-\tau),$$

where $h$ is the linear feedback kernel. $M_h$ is the memory length of the feedback process. In total, then, the model describes how temporal patterns of third order (i.e. the effects of triplets) for each input, and second order (i.e. the effects of pairs) for any of two interacting inputs, affect each output, taking into account differing noise levels and output spike-triggered feedback (the latter due to circuitry and/or membrane biophysics), and neuron-specific differences in thresholds.

Analyses included extraction of the first-, second- and third-order temporal firing within at least two defined minicolumns on MEAs inserted repetitively on multiple recording sessions in order to extract relevant patterns of minicolumnar activity related to successful image selection during the match phase of the task. The model defined inputs as intralaminar firing from neurons in L2/3 and outputs as intralaminar firing of L5 neurons, but the manner in which they were recorded determined the multicolumnar nature of the output patterns extracted by the MIMO model. In this manner, predictions of the L5 output related to the successful performance were monitored online during the task to define when successful trials were about to be completed by appropriate target selection as shown in figure 4. This online monitoring by the MIMO model provided the basis for interposing the correct L5 firing pattern as electrical pulses delivered to the same L5 recording pads of the MEAs in the same temporal interval of occurrence during match phase onset and completion of target selection (figures 2 and 4). Stimulation pulses consisted of biphasic constant-current square waves, 0.5 ms per phase, adjusted in intensity (10–50 $\mu$A) to produce local field potentials monitored on

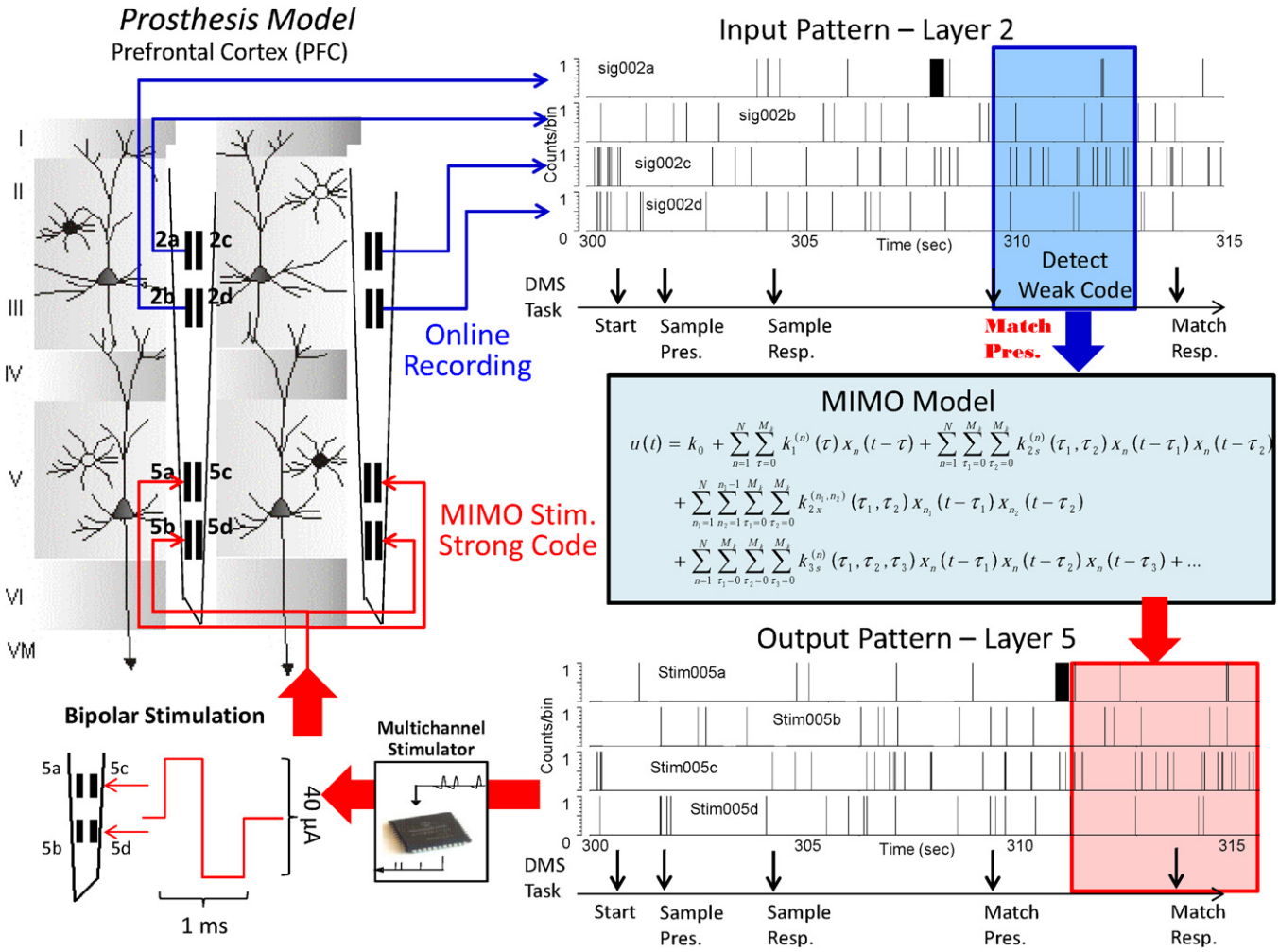


**Figure 4.** Integration of the MIMO model for calculating MR codes from L2/3 recordings and delivering output pulses to L5 recording pads to mimic strong codes during the DMS task. The schematic shows prefrontal cortical (PFC L2/3) recording and the NHP MIMO model with feedback stimulation applied to PFC L5. Neural recordings from layer 2/3 are analyzed to predict layer 5 neural activity, which is in turn used to generate stimulation patterns applied to layer 5 recording sites. MIMO model coefficients applicable to PFC recordings distinguish different features of the DMS task. This has provided the means to test the specificity of the MIMO codes recorded in L2/3 that occur on different types of trials (with different cognitive load) when applied as stimulation patterns to L5.

adjacent L5 recoding pads on the same and/or side-by-side implanted MEAs. Model-derived stimulation was applied on 30–50% of trials in each session to compare stimulated and non-stimulated trials in terms of correct performance. Effective stimulation patterns that were determined to facilitate performance under normal conditions were also applied at the same time during the trial, irrespective of prior L2/3 activity, when employed for the recovery of function during L2/3 to L5 activity (CCHs) was reduced pharmacologically as described below. In this manner, it was demonstrated that the MIMO model served as a prostheses for recovering decision making that required appropriate PFC columnar processing related to successful target selection in the DMS task.

### *Drug administration and dose*

Animals were trained to perform the task with IV saline injections into the vascular access port or sapphenous vein of the left leg prior to and midway through DMS testing sessions. A drug that has been shown to disrupt cognitive processing by altering dopamine reuptake in the PFC (Beveridge *et al* 2008, Tomasi *et al* 2010, Volkow *et al* 2005), cocaine (0.40 mg $kg^{-1}$) was administered (without cue) via IV injection midway through the session, replacing saline injections via the same route (Hampson *et al* 2011). The dose of the drug was adjusted, so that the animals continued to perform the task the remainder of the session such that the effects of the drug could be assessed on the columnar recordings in the first half of the session. Control saline injections were also administered in the second half of the session.

## Results

The NHPs ($n = 5$) were trained to perform the DMS (DMS; figure 1(A)) task (Hampson *et al* 2010, 2011, Porrino *et al* 2005) by making hand-tracking movements to different positions on the screen in front of them to obtain a juice reward for selection of the correct (sample) image, the location of which varied randomly in one of seven spatial positions on the

screen on each trial. Key variables in the task were the number of images (2–7) presented in the match phase, the duration of the delay (1–90 s), as well as the random placement of the sample image in the match phase (after the delay interval) that differed from the position responded to in the sample phase. In addition to incorporating key cognitive features such as attention, short-term memory, cognitive workload and reward expectancy, subjects were also executing a 'decision process' in the match phase (figure 1(A)) which involved 'target selection', i.e. a process that was related directly to neuron firing in the PFC (Hampson *et al* 2011).

### *Conformal assessment of PFC neural processing during match phase target selection*

The relevance of PFC activity to decision making has been investigated under several conditions in the past (Rao *et al* 1999, Goldman-Rakic 1996, Opris and Bruce 2005, Pesaran *et al* 2008, Resulaj *et al* 2009, Heekeren *et al* 2008, Opris *et al* 2011). Many of the prior reports of neural correlations with the executive function and decision making in a sensorimotor hierarchy (Miller and Cohen 2001, Pesaran *et al* 2008, Opris and Bruce 2005, Sugrue *et al* 2005) describe recordings from the area of the dorsolateral PFC (DLPFC) illustrated in figures 1(B)–(E), that have been shown to depend on the interaction between neurons in different layers within that same area of cortex (Weiler *et al* 2008, Kritzer and Goldman-Rakic 1995, Opris *et al* 2011). In this study, interlaminar connectivity was sensed by conformally-configured MEAs (figures 1(B)–(E)) positioned to simultaneously record PFC L2/3 and L5 neurons in adjacent 'minicolumns' during the performance of the DMS task as shown in figure 1(F). A demonstration of this type of columnar processing is shown in figures 2(A) and (B) for two PFC minicolumns recorded simultaneously with the MEA during the match phase of the task. This relationship was assessed for all recordings from MEAs in this study and the overall analysis was significant ($F_{(14,958)} = 2.73$, $p < 0.001$). Raster/PEHs for the two simultaneously recorded cell pairs (L2/3 and L5) at the indicated locations on the conformal MEA array positioned strategically in PFC (illustration in middle) showed significant increases in overall mean firing rates at the onset of the match phase ('M' onset = 0.0 s; pre versus post $F_{(1,958)} = 12.91$, $p < 0.001$) over the time (from 0.0 s to +2.0 s) in which arm movements involved in target selection were initiated (Hampson *et al* 2011, Porrino *et al* 2005). In addition, the L2/3 neurons shown in figures 2(A) and (B) (upper raster/PEHs) exhibited significantly higher overall mean firing rates ($F_{(1,958)} = 11.17$, $p < 0.001$) than the L5 neurons (lower raster/PEHs) recorded in minicolumns 1 and 2 on the MEA during the same phase of the task. However, to determine the fact that the firing of cell pairs in each vertical MEA recording array reflected columnar-based interlaminar communication, cross-correlations between vertically oriented cell pairs (minicolumns 1 and 2, figures 2(A) and (B)) were constructed to determine firing synchrony relative to the time of target presentation and selection in the match phase. The normalized CCHs in figure 2 depict differences in the correlation of L2/3 and L5 firing of the same cell pairs with respect to (1) the 'pre' match phase onset ($M = 0.0$) baseline (−2.0–0.0 s) versus 'post'-match phase onset (from 0.0 s to +2.0 s) after the presentation of images on the screen (figure 1(A)). The specificity of the cross-correlations between both L2/3 and L5 cell pairs (minicolumns 1 and 2) is shown in figures 2(A) and (B) by the overall significant increase in CCHs (figure 2(A): $F_{(1,401)} = 12.24$, $p < 0.001$; figure 2(B): $F_{(1,401)} = 15.14$, $p < 0.001$) during the performance of the Match response (green, Post-Match) relative to when the animal was waiting for the Delay interval to time out prior to image presentation (black, Pre-Match). This was supported by the fact that CCHs that compared cell pairs within the same L2/3 layer (not shown) or L2/3 cells within the same on one side of the MEA with the L5 cells on the opposite, diagonal-noncolumnar, side (figure 2(C)) did not exhibit a significant correlation ($F_{(1,401)} < 3.22$, $p > 0.10$).

### *Cognitive specificity of PFC columnar processing*

The relationship of columnar processing to cognitive performance of the DMS task was assessed by determining correlated firing between PFC L2/3 and L5 cell pairs in the Match phase of the task on correct versus error trials as shown in figure 3. Both the L2/3 and L5 cells showed increased firing during the Match phase on correct trials but reduced firing in that same task phase on trials in which the incorrect image was selected (figure 3(A), correct versus error trials). Figure 3(B) shows the mean (±SEM) firing rate change averaged over several PFC L2/3 and L5 cell pairs ($n = 60$) on correct versus error trials within the Match phase of trials in the same DMS sessions. Even though mean firing rates between 0.0 and +2.0 s were significantly higher for L2/3 than L5 cells ($F_{(1,958)} = 6.27$, $p < 0.01$), rate increases for both L2/3 and L5 cells were significantly lower on error versus correct trials (layer 2/3: $F_{(1,958)} = 11.12$, $p < 0.001$, layer 5: $F_{(1,958)} = 6.67$, $p < 0.01$). The distribution of match response latencies for both types of trials, correct (blue) versus error (red) trials, are shown in the histograms in figure 3(B) with the respective mean PEHs, indicating a difference in speed of movement that could reflect an increase related to performance in trials with increases in a number images (indicated below in figures 5(D) and 7 (F)). The significance of columnar firing for correct trials is also indicated in figure 3(C) by the decrease in correlated firing shown in the CCHs in error (red) versus correct (blue) trials for the same cell pair and over the same trials shown in figure 3(A). This same decrease in synchronous firing for mean normalized CCHs constructed for all the cell pairs ($n = 60$) in figure 3(B) on error trials, is shown in figure 3(D) which further validates the fact that firing between L2/3 and L5 cells was reduced in trials in which the wrong image was selected.

### *Application of the MIMO model facilitates columnar processing in PFC*

Prior investigations applying MIMO model-derived stimulation patterns to hippocampus in the rodent provided the means to enhance performance and overcome deficits induced by pharmacological treatments (Berger *et al* 2011). The same

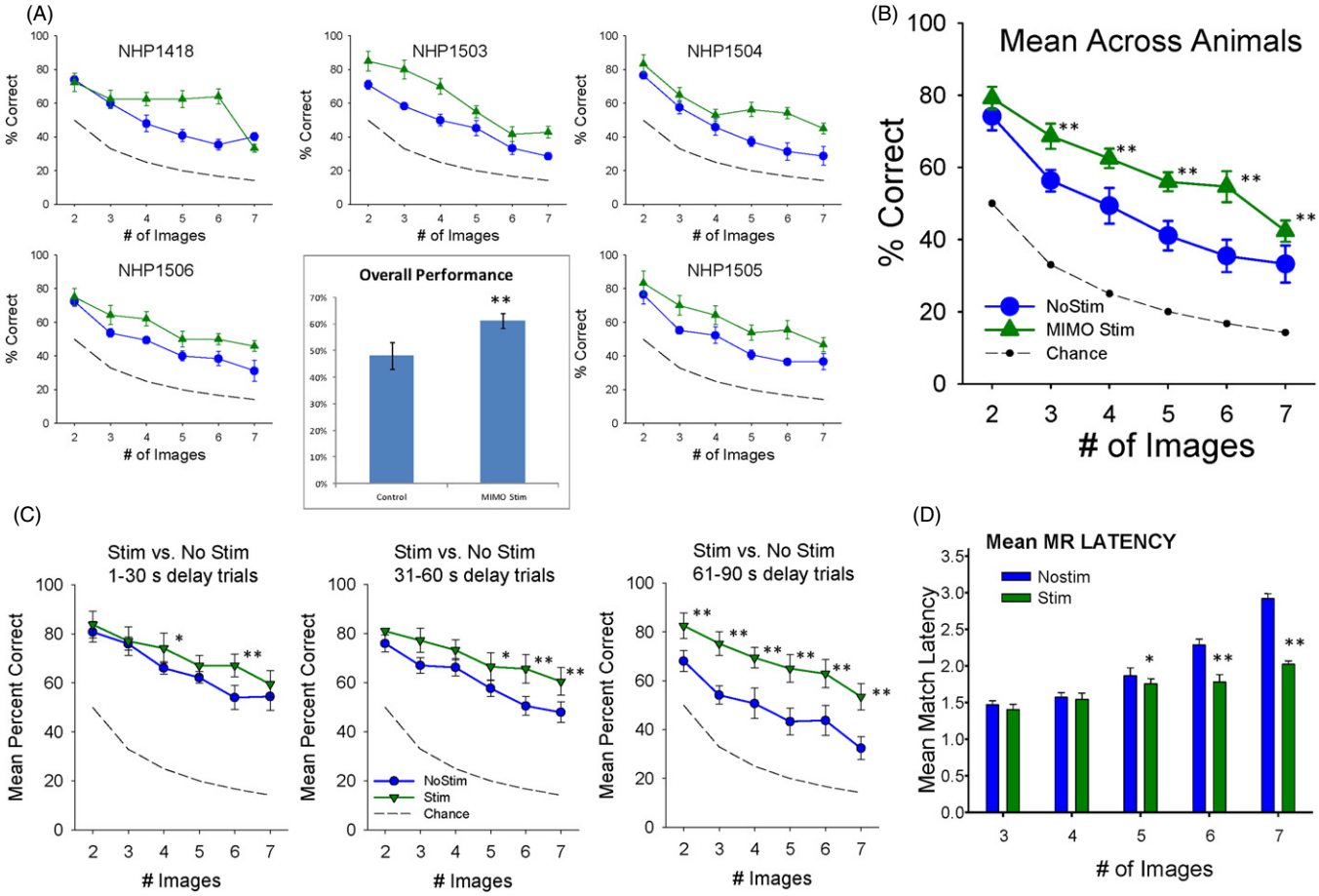


**Figure 5.** Facilitation of DMS performance by MIMO stimulation (A). MIMO stimulation applied to prefrontal cortex in five NHPs (indicated by number) performing the DMS task under normal conditions. The MIMO model was adapted to utilize L2/3 input to predict L5 output patterns delivered as electrical stimulation (figure 4) during target image selection in the match phase of the task (figure 1(A)). Each graph shows mean DMS performance ( ± SEM) as a function of trial complexity indicated by number of images (2–7) over 3–5 sessions comprised of ⩾120 trials per session. Performance is shown for normal trials in which stimulation was not delivered (no stimulation, No Stim) and trials in the same session in which the MIMO model-derived stimulation was delivered to the PFC L5 (MIMO stimulation) recording sites on MEAs for 2.0 s corresponding to limb movements associated with the match response. Dashed line indicates performance that could be achieved by random 'chance' selection at each degree of match difficulty related to the number of images to select from. Inset: average performance summed across trials, animals and sessions for no stimulation versus stimulation trials. $^{**}F_{(5,239)} > 42.16$, $p < 0.001$ increase compared to no stimulation. (B) Mean DMS performance as a function of images across all animals shown in (A) for stimulation versus no stimultaion trials. $^{**}F_{(1,239)} > 18.34$, $p < 0.001$ increase compared to no stimulation. (C) Effect of MIMO stimulation on DMS trials with differing delays as a function of number of images. Same results shown in (B) sorted by duration of trial delay prior to match phase onset (figure 1(A)) for no stimulation versus stimulation trials. $^{*}F_{(1,239)} > 8.22$, $p < 0.01$; $^{**}F_{(1,239)} > 13.40$, $p < 0.001$ increase compared to no stimulation. (D) Effect of MIMO stimulation on mean match response (MR) latency to respond to the match image on no stimulation versus stimulation trials. Mean ( ± SEM) latencies (in seconds) across animals and sessions as a function of number of images presented in the match phase. $^{*}F_{(1,239)} = 9.51$, $p < 0.01$; $^{**}F_{(1,239)} > 21.29$, $p < 0.001$ versus no stimulation.

MIMO model was applied in this study to multicolumnar PFC L2/3 and L5 cell pairs recorded during the Match phase of the DMS task. Spatiotemporal patterns associated with trials of correct performance were constructed from multiple ($n = 2$–4) simultaneously recorded confirmed MEA cell pairs in all NHPs ($n = 5$) tested. Derived L5 output firing associated with L2/3 input firing to the MIMO model, as shown in figure 4, was used to (a) predict performance on individual trials and (b) interject electrical stimulation patterns in L5 onto the same MEA pads from which predicted firing was extracted by the MIMO model. The effects of electrical stimulation patterns of several types including MIMO stimulation (figure 5) and control stimulation (figure 6) averaged over all NHPs and trials were significant ($F_{(59,239)} = 20.94$, $p < 0.001$, overall ANOVA). There was a significant effect of images ($F_{(5,239)} = 181.04$, $p < 0.001$) and stimulation ($F_{(9,239)} = 31.49$, $p < 0.001$) as well as the interaction (stim x images, $F_{(45,239)} = 1.65$, $p < 0.01$) as shown in figures 5 and 6. It is clear that MIMO stimulation facilitated performance above normal levels but was not consistent for the same types of trials in all animals (figure 5(A), individual NHPs); however, figure 5(B) shows that the overall mean effect of MIMO stimulation was to facilitate performance across trials with the increased number of images ($F_{(5,239)} = 42.16$, $p < 0.001$). Figure 5(C) shows the facilitatory effect of the MIMO-derived stimulation on trials with different delays and the number of images where performance on trials with longer delays (30–60 s, 61–90 s)

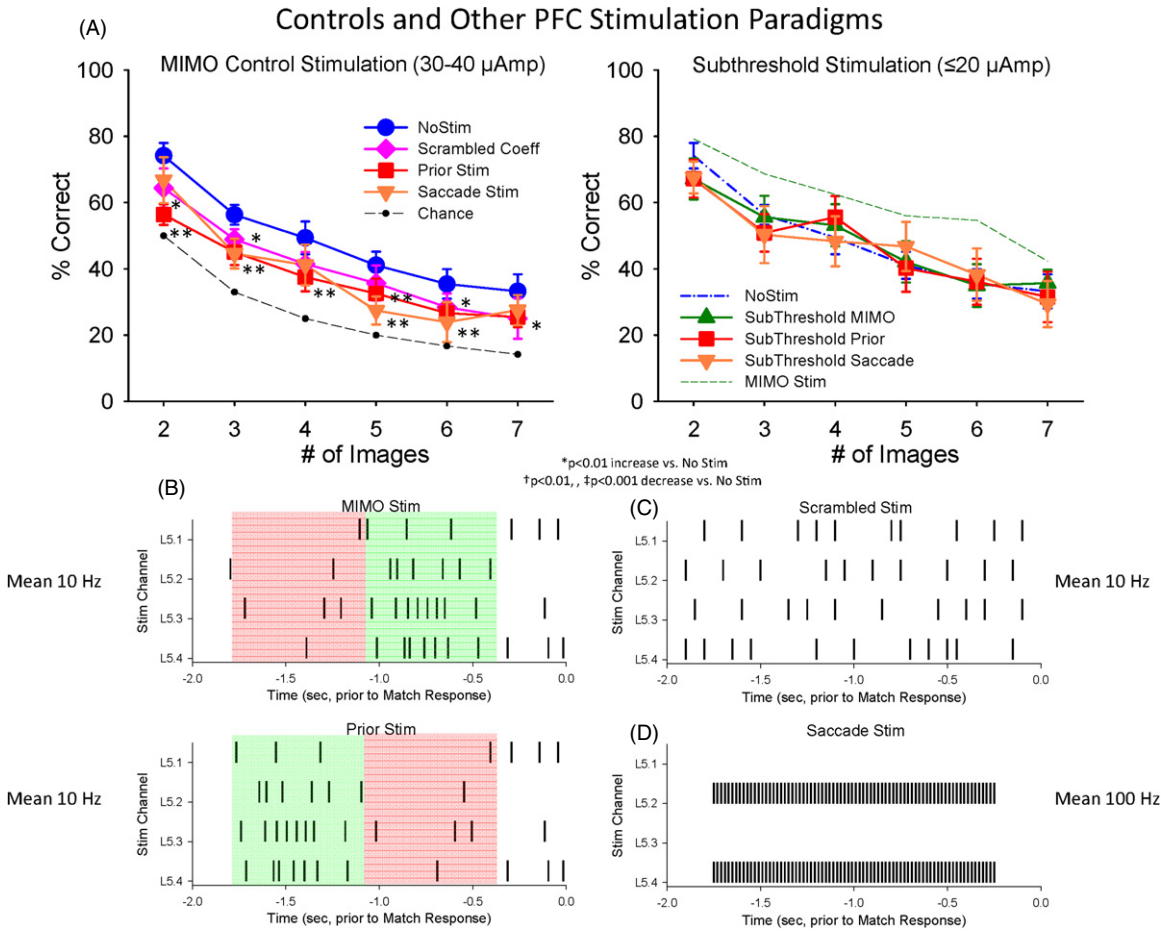


**Figure 6.** Lack of DMS facilitation by control stimulation paradigms which were not synchronized to MIMO-extracted PFC neuron firing. Mean ( ± SEM) DMS performance summed across all animals ($n = 5$) on trials with stimulation parameters and patterns (shown in (B) and (C)) that differed or were administered differently from those generated by the MIMO model (figure 5). (A) Left: mean DMS performance on trials with three different types of non-MIMO stimulation patterns (in (B)) delivered at the same intensity and pulse duration as MIMO stimulation (30–40 $\mu$A, 1 ms pulses) was decreased compared to control (no stimulation) performance. $^{*}F_{(1,239)} > 7.31$, $p < 0.01$; $^{**}F_{(1,239)} > 12.56$, $p < 0.001$ decrease versus no stimulation (No Stim). Right: DMS performance across animals on trials receiving the same non-MIMO stimulation patterns shown at left with reduced current levels ($\leqslant 20$ $\mu$A). Dotted green curve shows performance on trials with MIMO stimulation (figure 5)(B). (B) Prior stimulation pattern: the pattern consisted of the same stimulation channels and interstimulus intervals as the MIMO-derived stimulation pattern (MIMO Stim, top); however the early and late epochs of stimulation were inverted temporally such that stimulation that normally occurred synchronous with the match phase response was now delivered prior to the match response (prior stimulation, bottom). The illustration shows stimulation on a single trial in the match phase, contrasting MIMO stimulation patterns at the top in green starting 1.0 s after match phase onset (−2.0 s), with the control MIMO stimulation pattern starting at 0.25 s after match phase onset (bottom, in green) and terminating 1.0 s prior to the match phase response (0.0 s). (C) Scrambled stimulation with randomized MIMO coefficients and the same overall frequency and number of stimulation pulses as MIMO stimulation delivered in the same match phase time interval; (D) Saccade stimulation refers to stimulation associated with saccade generation with fixed frequency (100 Hz) delivered at the same intensity in the same match phase interval as MIMO stimulation (figure 5).

was less impaired on stimulated versus nonstimulated trials ($F_{(2,239)} = 13.49$, $p < 0.001$). Unlike the graded facilitation seen across trials as a function of the number of images (figure 5(A)), MIMO stimulation was equally effective ($F_{(2,239)} = 3.71$, $p > 0.05$) irrespective of the duration of delay (30–60 s, 61–90 s) prior to the onset of the match phase in the task (figure 5(B)). Finally, the facilitatory effects of MIMO stimulation on target selection and execution were strongly supported by a significant decrease ($F_{(4,401)} = 9.14$, $p < 0.01$) in the latency to make the match response (figure 5(D)) as a function of trial difficulty (number of images) on MIMO stimulation versus nonstimulation trials, which is consistent with figure 3(B) for differences in time of response execution on correct versus error trials.

### *Effects of control stimulation parameters show specificity of MIMO facilitation*

Because the effects of MIMO stimulation were so effective in facilitating performance (figure 5) several control measures were implemented to eliminate the possibility that mere addition of electrical pulses may have been the major factor for improved performance. One of the most obvious controls for the specificity of MIMO stimulation was to inject the same spatiotemporal stimulation pattern at a different time during the task to make sure that the derived multicolumnar L5 stimulation pattern was specific to when the decision to make the match response occurred on the trial. When the same MIMO pattern of stimulation at the same intensity was

delivered in the 1.0 s period prior to match phase onset, performance was actually significantly reduced ($F_{(5,239)} = 27.14$, $p < 0.001$) relative to non-stimulation levels as shown in figures 6(A) and (B). Another closely related control stimulation procedure involved the delivery of stimulation pulses to L5 in the same temporal relation to the MR but in a pattern with randomly scrambled MIMO coefficients (figure 6(C)) derived from online L2/3 activity (input pattern-layer 2, figure 4), which again, did not facilitate performance and actually decreased accuracy ($F_{(5,239)} = 13.95$, $p < 0.001$) across all trials (figure 6(A) scrambled). Another test for the specificity of MIMO stimulation was implemented using stimulation parameters previously shown to be effective for evoking saccades and improved performance in other cognitive tasks in NHPs (Opris *et al* 2005a, 2005b). These saccade-type stimulation parameters (figure 6(D)) delivered at the same intensity and in the same temporal interval as MIMO stimulation during the trial, did not facilitate performance and produced slight decreases in accuracy ($F_{(5,239)} = 19.13$, $p < 0.001$) similar to other control stimulation parameters shown in figure 6(A). As a final assessment of the relevance of stimulation intensity to these control stimulation patterns, pulses were reduced by 50% (<20 $\mu$A) and delivered in the same control stimulation patterns. Figure 6(A) (subthreshold stimulation) shows that not only did reducing stimulation intensity (a) not produce the facilitation of performance but also (b) eliminated the reduction in performance produced at the higher simulation intensities ($F_{(5,239)} < 0.52$, $p > 0.10$); which clearly indicates that the control stimulation parameters had an effect on neural tissue, but not the same facilitatory effect as columnar based, MIMO-derived stimulation.

### *Pharmacologic impairment of PFC columnar processing and DMS performance*

Extensive prior investigation of features that affect cognitive processing in DMS tasks have shown that Match phase activation of PFC is altered by the modulation of dopamine influences on task-related PFC cell firing by cocaine and other agents that alter dopamine uptake (Hampson *et al* 2011, Porrino *et al* 2005, Robbins and Arnsten 2009). To determine similar actions on PFC columnar activity in this task firing was assessed in the same minicolumns before and after the systemic injection of cocaine (0.40 mg kg$^{-1}$) midway through the DMS session. Figure 7(A) shows raster/PEHs for a PFC inter-laminar cell pair (L2/3 upper, L5 lower) recorded: (1) in the first 60 trials of a DMS session (Control) followed by, (2) the un-signaled administration (IV) of cocaine on trial 61 in the second half of the session for 60 more trials. It is clear that a significant reduction in match phase firing occurred in L2/3 ($F_{(1,958)} = 24.17$, $p < 0.001$) and L5 ($F_{(1,958)} = 19.72$, $p < 0.001$) in the cocaine versus control half of sessions (figure 7(A)), and that these changes in firing resembled closely the reductions shown for error trials in figures 3(A) and (B). The generality of this effect on match phase mean firing rate over a large population of cell pairs ($n = 30$) is shown in figure 7(B) as a significant decrease in the L2/3 cell activity ($F_{1,958)} = 13.43$, $p < 0.001$) relative to the saline half of the session. The reduction in L5 average firing rates in the cocaine half of the session approached but did not reach significance ($F_{(1,958)} = 1.48$, $p > 0.10$) which perhaps reflects decreased dopamine sensitive processes (Gulledge and Jaffe 1998) relative to L2/3 cells as has been indicated in prior studies of dopamine receptor actions in these PFC layers in NHPs (Bordelon-Glausier *et al* 2008, Robbins and Arnsten 2009). However, the more specific columnar firing indicator, CCHs for the single cell pair in figure 7(A) and for all cell pairs in figure 7(B) ($n = 30$) shown respectively in figures 7(C) and (D), indicate a clear decrease in correlated firing ($F_{(1,401)} > 11.22, p < 0.001$) after cocaine administration. The significance of this change with respect to cocaine's effect on columnar processing is shown in figure 7(E) as a scatter plot of correlation coefficients for the initial (control) and second (cocaine) half of cocaine administered sessions. Clearly, the lack of points on the diagonal line in the scatter plot indicates an alteration in synchronized firing in cell pairs that showed high correlation in firing during the first half of the session which was reduced to low levels after cocaine administration in the second half of the session (figure 7(E)). Finally, it is an important coincidence that the alterations in columnar processing produced by cocaine also influenced DMS performance in a manner consistent with the cognitive demand of the task. Figure 7(F) shows reduced mean performance accuracy as a function of the number of images presented in the match phase on trials presented during the cocaine half of the session ($F_{(5,239)} = 29.71$, $p < 0.001$) which confirms the graded effect as a function of trial difficulty and is also consistent with the lack of short latency MRs shown in figure 6(B). These data are supported by other findings showing impairment in the cognitive function by agents which altered activity in PFC (Arnsten 2000, Robbins and Arnsten 2009, Wang *et al* 2011) and agree with recent findings showing the involvement of neural activity in PFC as a function of difficulty of the trial (Hampson *et al* 2010).

### *MIMO stimulation-induced recovery of impaired DMS task performance*

Figures 5 and 6 show that MIMO L5 stimulation was exceedingly effective in facilitating DMS-task performance under normal conditions. This provided the basis for testing the effects of the MIMO model as a neuroprosthesis by interpolating stimulation of L5 on trials disrupted by cocaine injections during the session. It is clear from figure 7(E) that cocaine's overall effect was to alter PFC columnar firing in the same minicolumns that processed information effectively in the first half of the same session ($F_{(23,198)} = 18.65$, $p < 0.001$). Application of the MIMO model under these conditions (figure 8(A)) provided the means to detect non-effective trial specific firing in L2/3 cells which signaled the basis for concomitant delivery of L5 stimulation patterns associated with columnar firing patterns on successful trials shown to be facilitatory under normal conditions (figure 5). This online application, in which MIMO model controlled stimulation was delivered on trials during cocaine disrupted performance in the second half of the same session, was

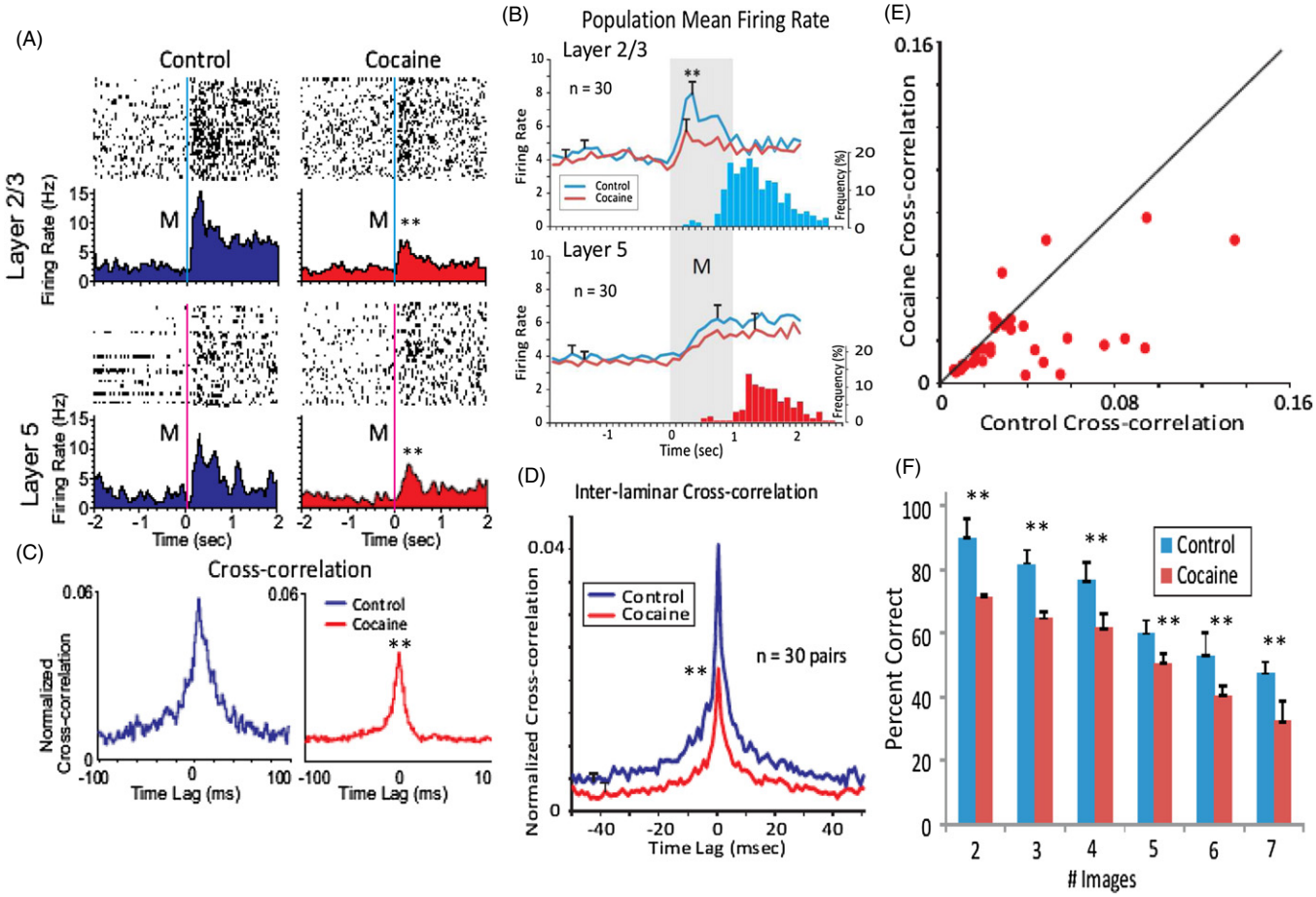


**Figure 7.** Pharmacological interruption of DMS-dependent inter-laminar processing. Effects of midsession cocaine administration (0.40 mg kg$^{-1}$ IV) on L2/3-L5 cell pair firing during performance of DMS task. (A): Rasters and PEHs show Match phase L2/3 and L5 inter-laminar activity as in figures 2 and 3 during the initial control (saline, blue) portion of the session and after cocaine administration (cocaine, red) midway through the same session. $^{**}F_{(1,958)} > 19.72$, $p < 0.001$ versus Control (saline). (B) Average PEHs for control (upper) versus cocaine trials (lower) summed over all inter-laminar L2/3 (blue) & L5 (red) PFC cell pairs ($n = 30$) recorded in the same sessions with cocaine administered at the midpoint (trial 62) of the session. Black (control) and green (cocaine) histograms show mean frequency distributions of latencies to make the MR relative to Match phase onset (M, 0.0 s). $^{*}F_{(1,958)} = 13.43$, $p < 0.001$ versus Control. (C) Cross-correlograms (CCHs) of firing between the L2/3 and L5 cell pair shown in (A) constructed from control trials ($n = 62$) in the first half of the session (blue-left), and after cocaine administration during the second half of the same session (red-right). $^{**}F_{(1,401)} = 17.22$, $p < 0.001$ versus Control. (D) Mean cross-correlation histograms (CCHs) for the same inter-laminar cell pairs ($n = 30$) shown in (B) constructed from trials in the control (blue) versus cocaine (red) halves of the session. $^{**}F_{(1,401)} = 11.22$, $p < 0.001$, versus Control. (E) Scatter plot of normalized cross-correlation coefficients from cell pairs shown in (D) for control (horizontal axis) and cocaine (vertical axis) halves of the same DMS sessions. Distribution of coefficients along the diagonal line would represent no change in correlation coefficients between the two halves of the session, whereas the demonstrated asymmetry of coefficient distribution reflects a significant change in inter-laminar correlated cell firing after cocaine administration. (F) Reduction in DMS (% correct) performance for all animals on trials with varying number of images (figures 5 and 6) for control versus cocaine segments of the same sessions ($n = 19$). $^{**}F_{(1,239)} > 16.01$, $p < 0.001$ Cocaine versus Control.

effective in reversing the detrimental effects of the drug (cocaine versus cocaine+MIMO Stim; $F_{(5,198)} = 15.05$, $p < 0.001$) across trials with 3–7 images (figure 8(B)). MIMO stimulation not only re-established control responding but also increased performance to the level achieved on stimulated trials (control versus drug+MIMO Stim, $F_{(5,198)} = 8.18$, $p < 0.001$) under saline-control conditions (figure 8(B)). Thus MIMO stimulation was more potent under conditions of cocaine-reduced columnar processing since it elevated mean performance from a markedly reduced level (relative to control performance) to a higher status that was slightly above control conditions ($F_{(5,198)} = 1.86$, $p > 0.10$, figure 8(B)); similar to the higher level achieved when the same stimulation was administered during baseline performance (figure 5). These results provide the first evidence that a neural prostheses in the MIMO model format can effectively reverse externally induced impairments in cortical function that directly influence cognitive processing in primate brain. The findings clearly demonstrate that the application of the MIMO model reversed the disruptive effects of cocaine on DMS performance ($F_{(5,198)} = 15.05$, $p < 0.001$) as shown in figure 8(C). This performance change after cocaine administration was shown to result directly from the reversal of reduced PFC inter-laminar processing in the same minicolumns to which successful MIMO L5 stimulation patterns were applied in the same session (figure 8(A)). Such

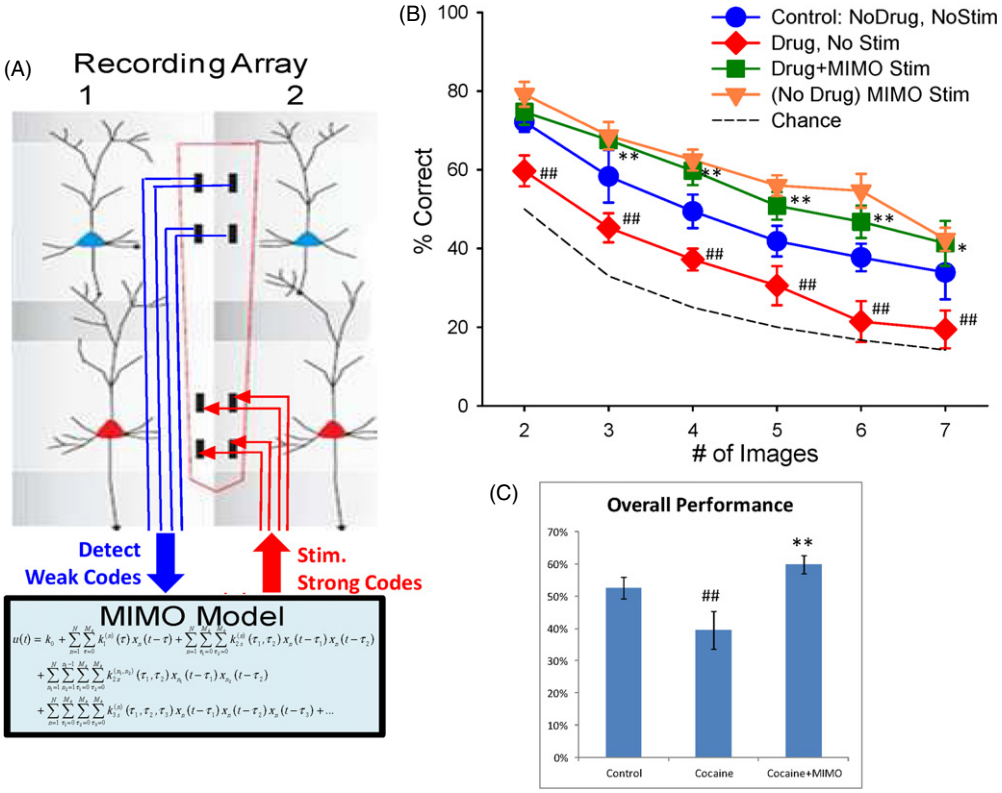


**Figure 8.** MIMO-based neural prosthetic recovery of PFC-dependent DMS performance. (A) Application of MIMO model detects increased 'weak code' L2/3 firing associated with error trials in DMS performance following cocaine exposure (figure 7). Output of the MIMO model is then utilized to stimulate L5 with a 'strong code' L5 pattern associated with correct (control) performance at the time of target selection in the match phase. (B) DMS performance resulting from MIMO stimulation applied to prefrontal cortex in five NHPs receiving split sessions in which each animal received saline injection prior to start of the behavioral sessions, and the received cocaine (0.4 mg kg$^{-1}$ IV) at the midpoint of the behavioral session. DMS mean ( $\pm$ SEM) performance during (1) control (no drug, No Stim) half of the session compared to (2) nonstimulated trials (drug, No Stim) in the cocaine half of the session and (3) MIMO stimulated (drug+MIMO Stim) trials in the cocaine half of the same session. Performance of MIMO stimulation trials in the absence of drug (figure 5) is also shown for comparison (no drug MIMO Stim). $^{\#\#}F_{(1,239)} > 16.82$, $p < 0.001$ decrease versus Control. $^{*}F_{(1,239)} = 7.22$, $p < 0.01$; $^{**}F_{(1,239)} > 10.63$, $p < 0.001$ increase versus Control. (C) Overall performance (mean $\pm$ SEM) shown for all animals on trials in (1) non-drug half of session (control), (2) cocaine half of session on trials with no stimulation (cocaine) and (3) cocaine half of session on trials with MIMO stimulation (cocaine+MIMO). $^{\#\#}F_{(5,239)} = 42.53$, $p < 0.001$; performance decrease versus control; $^{**}F_{(5,239)} > 15.05$, $p < 0.001$ performance increase versus control.

inherent determinants as well as the demonstrated specificity of the MIMO stimulation patterns in altering DMS performance (figures 5 and 6) provide evidence that the MIMO model effectively mimicked columnar information processing in PFC necessary to perform the DMS task.

## Discussion

### *Cognitive dependence on columnar processing in prefrontal cortex*

The findings in this study (figures 2, 3 and 5) are consistent with prior studies showing that neurons in the supra- and infra-granular layers of the PFC form efficient minicolumnar circuits during the selection/decision process in different experimental contexts (Weiler *et al* 2008, Takeuchi *et al* 2011). This decision-based columnar firing was demonstrated here during the match phase as required for the effective performance of this DMS task. The novel conformal ceramic recording probe (figures 1(E) and (F)) employed in this study allowed the assessment of inter-laminar correlated firing that was validated across sessions and animals in which multiple recordings of L2/3 and L5 cell pairs showed similar relations with respect to task-related as well as correlated firing in the match phase (figures 2, 3 and 7). A key variable in the DMS decision/selection process was the activation of multiple L5 neurons via the minicolumnar-related synchronous input from MEA-associated L2/3 neurons (represented as increased correlation in CCHs in figures 2, 3, 7), the latter of which have been shown to participate in the integration of sensory information via 'long-range' inputs from the dorsal visual stream in parietal/visual cortex (Resulaj *et al* 2009, Pesaran *et al* 2008, Opris and Bruce 2005). The functional significance of this measure of processing reflected by increased L2/3-to-L5 cross-correlation was validated directly via application of the nonlinear MIMO model to derive multicolumnar firing to define specific discharge patterns in L2/3 related to L5 firing under conditions of successful performance. Since this relationship was a direct spatiotemporal reflection of the increased inter-laminar firing shown by the same identified cell pairs, it provides independent validation that the extracted activity associated with correct decision making and target

selection characterized by the MIMO model was in fact columnar specific. Further demonstration of the accuracy of this characterization of firing by the MIMO model was empirically demonstrated by the interposed stimulation of L5 recording areas with streams of pulses that mimicked the MIMO extracted L5 spatiotemporal firing patterns that (1) facilitated performance under normal testing conditions on stimulated versus nonstimulated trials (figures 4 and 5) and (2) also recovered performance decreased by drug-reduced columnar firing following cocaine administration in the same session (figures 7 and 8).

*Successful performance related to PFC columnar processing*

Figure 3 shows that on correct versus error trials, processing of columnar information was related to significant increases in the cross-correlation of firing between L2/3 and L5 PFC cell pairs during image presentation on the screen in the match phase of the DMS task. This close correspondence between columnar firing and cognitive processing was confirmed by administering cocaine midway through the test session which simultaneously decreased correlated inter-laminar firing in identified cell pairs (figures 7(A)–(F) as well as reduced task performance (figure 7(G)) over the same time frame of the session. The scatter plot in figure 7(E) shows that the reduced inter-laminar firing produced by cocaine was most extreme for cell pairs that exhibited a high degree of correlation in the normal (saline control) half of the session, while cell pairs with low initial normalized correlation coefficients (<0.04), were relatively unaffected by cocaine administration. This supports the view that graded levels of cognitive output may be related to the degree or intensity of columnar activity on a given trial (van Veluw *et al* 2012, Buxhoeveden *et al* 2006). These findings are in complete agreement with prior studies showing marked influences of acute administered cocaine in altering task-related neural firing (Hampson *et al* 2011, Opris *et al* 2009, Stuber *et al* 2005) and support the possibility that cocaine-influenced dopaminergic modulation of PFC neurons was responsible for regulating columnar activity in a manner that varies with decision making in humans exposed to the same drug (Tomasi *et al* 2010, Volkow *et al* 2005).

*Facilitation of cognitive performance via MIMO model columnar stimulation*

The effectiveness of the MIMO-derived multicolumnar stimulation of L5 neurons in this task provides an important insight into the microcircuit nature of PFC activity related to decision making and target selection during the DMS task (figures 1(A) and 2). The MIMO model derived columnar stimulation pattern (figure 4) was shown to be critical for facilitation of task performance (figures 5 and 8) because of the ineffectiveness of other forms of stimulation delivered to the same loci at the same or reduced intensities but in different patterns and frequencies during the execution of the match response (figure 6). Even more specificity was provided by showing that the same effective MIMO-derived stimulation patterns, but delivered prior to the time at which movement initiation and target selection occurred within the match phase of the task (figure 6(B), 'prior stimulation'). The specific nature of MIMO facilitation was also exhibited by the reduced latency to select the correct image, but only on the more difficult trials in which latencies were increased more under nonstimulation conditions (figure 5).

The neural prosthesis presented here differs from prior studies to develop prostheses and brain-machine interfaces in humans, since neural interfaces have typically consisted of sensory input and/or motor output systems (Jackson and Fetz 2011, Laczko 2011, Lebedev and Nicolelis 2011), each of which is 'anchored' to a physical event of some type (i.e. receptor activation or limb movement). Basic sensory inputs, such as cochlear (Shannon 2012) or retinal implants (Weiland *et al* 2011) have employed neural stimulation as utilized here, but only as a replacement of sensory inputs, not for cognitive processing of that input. On the other hand, motor cortical prosthetics are primarily output devices which typically utilize neural signals in motor and premotor areas for the control of movement of a robotic limb (Judy 2012, van Hemmen and Schwartz 2008, Hochberg *et al* 2012). More recently, attempts to integrate 'haptic' feedback into limb prosthetics has resulted in devices which stimulate somatosensory and thalamic neurons to provide tactile and proprioceptive feedback information to the brain to 'close the loop' on motor processing (Weber *et al* 2011, Hatsopoulos and Suminski 2011, O'Doherty *et al* 2012). In contrast to these above approaches, the nonlinear MIMO neuroprosthesis described here bypasses the cortico-spinal and thalamo-cortical systems for limb control by directly influencing motor control decisions via columnar stimulation in PFC (Miller and Cohen 2001, Graybiel 2008, Laczko 2011). In addition, the sensory information processed is neither primary nor proprioceptive since the input assessed by the MIMO model was from the inter-laminar layer 2 which receives pre-processed information from other brain regions (Weiler *et al* 2008, Mountcastle 1997). The results therefore demonstrate that prefrontal minicolumns represent and control specific cognitive decisions within the DMS task, and that MIMO-derived stimulation, delivered during the match phase, selectively enhanced correct decisions at a higher cognitive level than strict motor control.

*MIMO model induced recovery from cocaine altered cognitive processing*

Prior applications of MIMO models to disrupted neural processing in rodent hippocampus established the functional basis for employing this approach in the design and implementation of the cortical neuroprostheses demonstrated here (Berger *et al* 2012, Hampson *et al* 2012a, Hampson *et al* 2012b, Berger *et al* 2011). What is presented here is the first application of the MIMO model to primate brain via a conformal electrode MEA capable of extracting spatiotemporal neural firing patterns related to known underlying columnar microcircuitry in PFC, which not only extends application of the MIMO model to other brain areas but also to the performance of human-like cognitive tasks. The recovery from cocaine-induced disruption shown

in figure 8 utilized the MIMO model to (1) extract, characterize and predict spatiotemporal patterns critical for effective performance and (2) interpose those same patterns into layer 5 using multichannel electrical stimulation. This constitutes the direct application of a device that mimics local circuit (multicolumnar activation) operation to restore cognitive processing shown to depend on the same columnar-based firing under normal conditions (figure 3). Also, in contrast to prior successful applications of MIMO model stimulation (Hampson *et al* 2012a, Berger *et al* 2011), the extent and range of effectiveness in improving and recovering performance (figures 5 and 7) was much greater in this task. However, what is of major importance in regard to this neuroprosthetics demonstration is the fact that effective L5 stimulation parameters had to mimic those derived by the MIMO model reflecting L2/3–L5 multicolumnar spatiotemporal firing sampled on the MEAs under normal circumstances. This was confirmed by stimulating the same MEA sites with different patterns or frequencies of pulses at the same intensities (figure 6), which were not only ineffective, but in most cases disrupted normal task performance. Therefore the stimulation patterns extracted by the MIMO model were not only specific, because they reflected firing on successful trials, they also increased performance above control levels, because the latter included more trials on which ineffective processing, (i.e. errors) occurred during the session (figures 3, 6 and 8).

## Conclusions

These unique results show that columnar interactions between prefrontal neurons that encode and process information relevant to executive function and decision making (Goldman-Rakic 1996, Opris and Bruce 2005, Heekeren *et al* 2008, Opris *et al* 2005b) are necessary for the successful performance of this DMS task (figures 2 and 3), and are capable of being simulated and interposed to facilitate and recover performance via application of a MIMO model-based neuroprosthesis, as demonstrated here. Since the possible neural basis for effective performance in this task relates to significant increased transmission within PFC minicolumns to select relevant cues during target presentation (figure 3), interposing a MIMO model to control this type of processing provides a means of reducing random fluctuations in performance under normal conditions. It was also possible to re-establish appropriate task-dependent processing under circumstances in which performance was impaired by factors that modulate the degree of columnar firing such as cocaine administration (figures 7 and 8). In addition to provide a potential insight into other types of cognitive impairments involving decision making and executive function in the human brain as a result of disease or injuries (Brennan and Arnsten 2008, Dobbs 2010, Duncan *et al* 1997, Shallice and Burgess 1991, Wang *et al* 2011, Casanova *et al* 2010), these results provide confirmation that a MIMO-based functional device, if properly integrated with normal brain operation, as provided by the conformal MEAs used here, can recover and even improve performance in complex tasks via simulation of columnar processing as a means of overcoming impaired cognitive function in the primate brain.

## Acknowledgments

We thank Joshua Long, Joseph Noto, Brian Parish, Joshua Fuqua, Mack Miller, and Shahina Kozhisseri for their assistance on this project. This work was supported by NIDA grants DA06634, DA023573 & DA026487, and Defense Advanced Research Projects Agency (DARPA) contract N66601-09-C-2080 to SAD; by NIH/NIBIB Grant P41-EB001978 to VZM; and by NSF grant EEC-0310723, and DARPA contract N66601-09-C-2081 to TWB.

## References

Arnsten A F 2000 Stress impairs prefrontal cortical function in rats and monkeys: role of dopamine D1 and norepinephrine alpha-1 receptor mechanisms *Prog. Brain Res.* **126** 183–92

Baddeley A 2002 Fractionating the central executive *Principles of Frontal Lobe Function* ed D T Stuss and R T Knight (New York: Oxford University Press) pp 246–60

Berger T W *et al* 2005 Restoring lost cognitive function *IEEE Eng. Med. Biol. Mag.* **24** 30–44

Berger T W, Hampson R E, Song D, Goonawardena A, Marmarelis V Z and Deadwyler S A 2011 A cortical neural prosthesis for restoring and enhancing memory *J. Neural Eng.* **8** 046017

Berger T W, Song D, Chan R H M, Marmarelis V Z, LaCoss J, Wills J, Hampson R E, Deadwyler S A and Granacki J J 2012 A hippocampal cognitive prosthesis: multi-input, multi-output nonlinear modeling and VLSI instrumentation *IEEE Trans. Neural Syst. Rehabil. Eng.* **20** 198–211

Beveridge T J, Gill K E, Hanlon C A and Porrino L J 2008 Review. Parallel studies of cocaine-related neural and cognitive impairment in humans and monkeys *Phil. Trans. R. Soc.* **363** 3257–66

Bordelon-Glausier J R, Khan Z U and Muly E C 2008 Quantification of D1 and D5 dopamine receptor localization in layers I, III, and V of *Macaca mulatta* prefrontal cortical area 9: coexpression in dendritic spines and axon terminals *J. Comp. Neurol.* **508** 893–905

Brennan A R and Arnsten A F 2008 Neuronal mechanisms underlying attention deficit hyperactivity disorder: the influence of arousal on prefrontal cortical function *Ann. New York Acad. Sci.* **1129** 236–45

Buxhoeveden D P and Casanova M F 2002 The minicolumn hypothesis in neuroscience *Brain* **125** 935–51

Buxhoeveden D P, Semendeferi K, Buckwalter J, Schenker N, Switzer R and Courchesne E 2006 Reduced minicolumns in the frontal cortex of patients with autism *Neuropathol. Appl. Neurobiol.* **32** 483–91

Casanova M F, El-Baz A, Vanbogaert E, Narahari P and Switala A 2010 A topographic study of minicolumnar core width by lamina comparison between autistic subjects and controls: possible minicolumnar disruption due to an anatomical element in-common to multiple laminae *Brain Pathol.* **20** 451–8

Casanova M F, Kreczmanski P, Trippe J, Switala A, Heinsen H, Steinbusch H W and Schmitz C 2008 Neuronal distribution in the neocortex of schizophrenic patients *Psychiatry Res.* **158** 267–77

Deadwyler S A, Porrino L, Siegel J M and Hampson R E 2007 Systemic and nasal delivery of orexin-A (hypocretin-1) reduces the effects of sleep deprivation on cognitive performance in nonhuman primates *J. Neurosci.* **27** 14239–47

Dobbs D 2010 Schizophrenia: the making of a troubled mind *Nature* **468** 154–6

Duncan J, Johnson R, Swales M and Freer C 1997 Frontal lobe deficits after head injury: unity and diversity of function *Cogn. Neuropsychol.* **14** 713–41
Gold J I and Shadlen M N 2007 The neural basis of decision making *Annu. Rev. Neurosci.* **30** 535–74
Goldman-Rakic P S 1996 The prefrontal landscape: implications of functional architecture for understanding human mentation and the central executive *Phil. Trans. R. Soc.* **351** 1445–53
Grabenhorst F, Rolls E T and Parris B A 2008 From affective value to decision-making in the prefrontal cortex *Eur. J. Neurosci.* **28** 1930–9
Graybiel A M 2008 Habits, rituals, and the evaluative brain *Annu. Rev. Neurosci.* **31** 359–87
Gulledge A T and Jaffe D B 1998 Dopamine decreases the excitability of layer V pyramidal cells in the rat prefrontal cortex *J. Neurosci.* **18** 9139–51
Hampson R E, Coates T D Jr, Gerhardt G A and Deadwyler S A 2004a Ceramic-based microelectrode neuronal recordings in the rat and monkey *EMBS: Proc. Annu. Int. Conf. of the IEEE Engineering in Medicine and Biology Society* vol 25 pp 3700–3
Hampson R E, Opris I and Deadwyler S A 2010 Neural correlates of fast pupil dilation in nonhuman primates: relation to behavioral performance and cognitive workload *Behav. Brain Res.* **212** 1–11
Hampson R E, Pons T P, Stanford T R and Deadwyler S A 2004b Categorization in the monkey hippocampus: a possible mechanism for encoding information into memory *Proc. Natl Acad. Sci. USA* **101** 3184–89
Hampson R E, Porrino L J, Opris I, Stanford T and Deadwyler S A 2011 Effects of cocaine rewards on neural representations of cognitive demand in nonhuman primates *Psychopharmacology (Berl)* **213** 105–18
Hampson R E, Song D, Chan R H M, Sweatt AJ, Fuqua J, Gerhardt GA, Shin D, Marmarelis VZ, Berger TW and Deadwyler SA 2012a A nonlinear model for hippocampal cognitive prostheses: memory facilitation by hippocampal ensemble stimulation *IEEE Trans. Neural Syst. Rehabil. Eng.* **20** 184–97
Hampson R E, Song D, Chan R H M, Sweatt A J, Riley M R, Goonawardena A V, Marmarelis V Z, Gerhardt G A, Berger T W and Deadwyler S A 2012b Closing the loop for memory prosthesis: Detecting the role of hippocampal neural ensembles using nonlinear models *IEEE Trans. Neural Syst. Rehabil. Eng.* **20** 510–25
Hansen BJ and Dragoi V 2011 Adaptation-induced synchronization in laminar cortical circuits *Proc. Natl Acad. Sci. USA* **108** 10720–5
Hasselmo M E 2005 A model of prefrontal cortical mechanisms for goal-directed behavior *J. Cogn. Neurosci.* **17** 1115–29
Hatsopoulos N G and Suminski A J 2011 Sensing with the motor cortex *Neuron* **72** 477–87
Heekeren H R, Marrett S and Ungerleider L G 2008 The neural systems that mediate human perceptual decision making *Nat. Rev. Neurosci.* **9** 467–79
Hochberg L R *et al* 2012 Reach and grasp by people with tetraplegia using a neurally controlled robotic arm *Nature* **485** 372–5
Jackson A and Fetz E E 2011 Interfacing with the computational brain *IEEE Trans. Neural Syst. Rehabil. Eng.* **19** 534–41
Judy J W 2012 Neural interfaces for upper-limb prosthesis control: opportunities to improve long-term reliability *IEEE Pulse* **3** 57–60
Kritzer M F and Goldman-Rakic P S 1995 Intrinsic circuit organization of the major layers and sublayers of the dorsolateral prefrontal cortex in the rhesus monkey *J. Comp. Neurol.* **359** 131–43
Kusunoki M, Sigala N, Nili H, Gaffan D and Duncan J 2010 Target detection by opponent coding in monkey prefrontal cortex *J. Cogn. Neurosci.* **22** 751–60
Laczko J 2011 Modeling of human movements, neuroprostheses *Ideggyogy Sz.* **64** 229–33
Lebedev M A and Nicolelis M A 2011 Toward a whole-body neuroprosthetic *Prog. Brain Res.* **194** 47–60
Marmarelis V Z, Shin D C, Song D, Hampson R E, Deadwyler S A and Berger T W 2011 Dynamic nonlinear modeling of interactions between neuronal ensembles using principal dynamic modes *Conf. Proc. IEEE Eng. Med. Biol. Soc.* **2011** 3334–7
Miller E K and Cohen J D 2001 An integrative theory of prefrontal cortex function *Annu. Rev. Neurosci.* **24** 167–202
Miyaki A, Friedman N, Emerson M, Witzki A, Howerter A and Wagner T 2000 The unity and diversity of executive functions and their contributions to complex frontal lobe tasks: a latent variable analysis *Cogn. Psychol.* **41** 49–100
Mo J, Schroeder C E and Ding M 2011 Attentional modulation of alpha oscillations in macaque inferotemporal cortex *J. Neurosci.* **31** 878–82
Mountcastle V B 1997 The columnar organization of the neocortex *Brain* **120** 701–22
Moxon K A, Leiser S C, Gerhardt G A, Barbee K A and Chapin J K 2004 Ceramic-based multisite electrode arrays for chronic single-neuron recording *IEEE Trans. Biomed. Eng.* **51** 647–56
O'Doherty J E, Lebedev M A, Li Z and Nicolelis M A 2012 Virtual active touch using randomly patterned intracortical microstimulation *IEEE Trans. Neural Syst. Rehabil. Eng.* **20** 85–93
Opris I, Barborica A and Ferrera V P 2005a Effects of electrical microstimulation in monkey frontal eye field on saccades to remembered targets *Vis. Res.* **45** 3414–29
Opris I, Barborica A and Ferrera V P 2005b Microstimulation of the dorsolateral prefrontal cortex biases saccade target selection *J. Cogn. Neurosci.* **17** 893–904
Opris I and Bruce C J 2005 Neural circuitry of judgment and decision mechanisms *Brain Res. Brain Res. Rev.* **48** 509–26
Opris I, Hampson R E and Deadwyler S A 2009 The encoding of cocaine versus natural rewards in the striatum of nonhuman primates: categories with different activations *Neuroscience* **163** 195–204
Opris I, Hampson R E, Stanford T R, Gerhardt G A and Deadwyler S A 2011 Neural activity in frontal cortical cell layers: evidence for columnar sensorimotor processing *J. Cogn. Neurosci.* **23** 1507–21
Pesaran B, Nelson M J and Andersen R A 2008 Free choice activates a decision circuit between frontal and parietal cortex *Nature* **453** 406–9
Porrino L J, Daunais J B, Rogers G A, Hampson R E and Deadwyler S A 2005 Facilitation of task performance and removal of the effects of sleep deprivation by an ampakine (CX717) in nonhuman primates *PLoS Biol* **3** e299
Porrino L J, Smith H R, Nader M A and Beveridge T J 2007 The effects of cocaine: a shifting target over the course of addiction *Prog. Neuropsychopharmacol. Biol. Psychiatry* **31** 1593–600
Posner M and Snyder C 1975 Attention and cognitive control *Information Processing and Cognition: The Loyola Symposium* ed R Solso (Hillsdale, NJ: L Erlbaum Assoc.)
Rao S G, Williams G V and Goldman-Rakic P S 1999 Isodirectional tuning of adjacent interneurons and pyramidal cells during working memory: evidence for microcolumnar organization in PFC *J. Neurophysiol.* **81** 1903–16
Resulaj A, Kiani R, Wolpert D M and Shadlen M N 2009 Changes of mind in decision-making *Nature* **461** 263–6
Robbins T W and Arnsten A F 2009 The neuropsychopharmacology of fronto-executive function: monoaminergic modulation *Annu. Rev. Neurosci.* **32** 267–87
Shallice T and Burgess P 1996 The domain of supervisory processes and temporal organization of behaviour *Philos. Trans. R. Soc.* **351** 1405–11
Shallice T and Burgess P W 1991 Deficits in strategy application following frontal lobe damage in man *Brain* **114** 727–41

Shannon R V 2012 Advances in auditory prostheses *Curr. Opin. Neurol.* **25** 61–6

Song D, Chan R H, Marmarelis V Z, Hampson R E, Deadwyler S A and Berger T W 2007 Nonlinear dynamic modeling of spike train transformations for hippocampal-cortical prostheses *IEEE Trans. Biomed. Eng.* **54** 1053–66

Song D, Chan R H, Marmarelis V Z, Hampson R E, Deadwyler S A and Berger T W 2009 Nonlinear modeling of neural population dynamics for hippocampal prostheses *Neural Netw.* **22** 1340–51

Stuber G D, Roitman M F, Phillips P E, Carelli R M and Wightman R M 2005 Rapid dopamine signaling in the nucleus accumbens during contingent and noncontingent cocaine administration *Neuropsychopharmacology* **30** 853–63

Sugrue L P, Corrado G S and Newsome W T 2005 Choosing the greater of two goods: neural currencies for valuation and decision making *Nat. Rev. Neurosci.* **6** 363–75

Takeuchi D, Hirabayashi T, Tamura K and Miyashita Y 2011 Reversal of interlaminar signal between sensory and memory processing in monkey temporal cortex *Science* **331** 1443–7

Tomasi D, Volkow N D, Wang R, Carrillo J H, Maloney T, Alia-Klein N, Woicik PA, Telang F and Goldstein R Z 2010 Disrupted functional connectivity with dopaminergic midbrain in cocaine abusers *PLoS One* **5** e10815

van Hemmen J L and Schwartz A B 2008 Population vector code: a geometric universal as actuator *Biol. Cybern.* **98** 509–18

van Veluw S J, Sawyer E K, Clover L, Cousijn H, De J C, Esiri M M and Chance S A 2012 Prefrontal cortex cytoarchitecture in normal aging and Alzheimer's disease: a relationship with IQ *Brain Struct. Funct.* doi:10.1007/s00429-012-0381-x, PMID: 22302432

Volkow N D, Wang G J, Ma Y, Fowler J S, Wong C, Ding Y S, Hitzemann R, Swanson J M and Kalivas P 2005 Activation of orbital and medial prefrontal cortex by methylphenidate in cocaine-addicted subjects but not in controls: relevance to addiction *J. Neurosci.* **25** 3932–9

Wang M, Gamo N J, Yang Y, Jin L E, Wang X J, Laubach M, Mazer J A, Lee D and Arnsten A F 2011 Neuronal basis of age-related working memory decline *Nature* **476** 210–3

Weber D J, London B M, Hokanson J A, Ayers C A, Gaunt R A, Torres R R, Zaaimi B and Miller L E 2011 Limb-state information encoded by peripheral and central somatosensory neurons: implications for an afferent interface *IEEE Trans. Neural Syst. Rehabil. Eng.* **19** 501–13

Weiland J D, Cho A K and Humayun M S 2011 Retinal prostheses: current clinical results and future needs *Ophthalmology* **118** 2227–37

Weiler N, Wood L, Yu J, Solla S A and Shepherd G M 2008 Top-down laminar organization of the excitatory network in motor cortex *Nature Neurosci.* **11** 360–6